SCIENTIFIC REPORTS

OPEN

SUBJECT AREAS:
SYNTHESIS AND PROCESSING
MATERIALS FOR ENERGY AND CATALYSIS

Received
10 June 2014

Accepted
18 August 2014

Published
12 September 2014

Correspondence and requests for materials should be addressed to Y.W. (chemwy@zju.edu.cn)

Design and Fabrication of Hierarchically Porous Carbon with a Template-free Method

Yutong Gong, Zhongzhe Wei, Jing Wang, Pengfei Zhang, Haoran Li & Yong Wang

Carbon Nano Materials Group, ZJU-NHU United R&D Center, Center for Chemistry of High-Performance and Novel Materials, Key Lab of Applied Chemistry of Zhejiang Province, Department of Chemistry, Zhejiang University, 310028 Hangzhou, P. R. China.

Fabrication of hierarchically porous carbon materials (HPCs) with high surface area and pore volume has always been pursued. However, the currently effective template methods and acid/base activation strategies suffer from the drawbacks of either high costs or tedious steps. Herein, HPCs with 3D macro-mesopores and short-range meso-micropores were fabricated via an easy and sustainable two-step method from biomass. Macro-mesopores were constructed by slightly accumulation/aggregation of carbon spheres ranging from 60 nm to 80 nm, providing efficient mass diffusion pathways. Short-range mesopores and micropores with high electrolyte accessibility were developed in these spheres by air activation. The obtained HPCs showed surface area values up to 1306 m^2/g and high mesopore volume proportion (63.9%). They demonstrated excellent capacitance and low equivalent series resistance (ESR) as supercapacitor electrode materials, suggesting the efficient diffusion and adsorption of electrolyte ions in the designed hierarchically porous structure.

Design and fabrication of nanoporous carbon materials have attracted great interest due to their practical or potential applications in catalysis, adsorption, drug delivery, and energy storage as well as conversion[1–4]. In general, the diffusion and adsorption of reactants or ions in nanopores are the two main factors determining the performance of carbon materials. Therefore, developing porous carbon materials with proper adsorption capability and efficient diffusion path is of great significance.

Mesoporous carbon materials with pore size between 2 nm ~ 50 nm have been attached great attention because mesopores offer effective transmission path for reaction substrates with moderate accessible surface area. Lots of extraordinary works described the synthesis of highly ordered mesoporous carbon materials via hard- or soft-template methods[5–8]. In common, hard-template methods always suffer from the drawbacks such as the massive use of template agents and tedious template removal processes. As for soft-template strategies, the experimental conditions universally need to be very precise at low carbon precursor concentration, which hinders the mass production[9,10]. The mesopores developed by template methods are always two-dimensional and long-range, which results in long transportation distance.

Hierarchically porous materials show great priority in practical applications because they combine the advantages of the pores with different sizes. Macropores (diameter >50 nm) can serve as buffering micro-reservoirs that minimize diffusion distances. Short-range mesopores could provide larger accessible surface area and smaller ion-transport resistance. Micropores (diameter <2 nm) hold the advantages of shape-selectivity and size-selectivity for guest molecules. They also supply high surface area together with strong adsorption ability[11]. Over the past years, many works have been reported to fabricate HPCs with macro-mesopores or meso-micropores[12–16]. For example, much effort has been spent on the fabrication of hierarchically porous carbon aerogels by Antonietti *et al* via hydrothermal carbonization (HTC) of carbohydrates[17,18]. Although the process is sustainable, the freeze-drying step is inevitable to maintain the hierarchical pores, which makes this technique time-consuming. The BET surface area and pore volume still have much space to improve even after activation at high temperatures. Some synthetic strategies of hierarchically porous SiO_2 were extended to the fabrication of porous carbon materials by using phloroglucinol or phenol/formaldehyde as carbon precursor and a soft block copolymer as mesopore template[19,20]. However, they can't be transplanted to the HTC of carbohydrates because the block copolymer micelles are typically unstable at the HTC temperature (*e.g.* D-Glucose, 180°C)[9,21]. Very recently, Zhao and Qiao *et al* reported the synthesis of mesoporous carbon spheres ranging from 80 nm to 400 nm. After 12 hours of heat treatment in N_2 atmospheres, the HPCs with high surface area were developed[22]. This method

still involves the massive use of soft templates and organic solvents. Therefore, the discovery of sustainable and easy methods for the production of HPCs is still in great demand.

Herein, we reported a novel and large scale synthetic method for the production of HPCs with 3D macro-mesopores and short-range meso-micropores (Figure S1). Tiny amount of commercial available kayexalate (< 1% to carbohydrate) was employed as a structure-directing agent during the HTC of carbohydrates. The 3D macro-mesoporous nanostructure was constructed by slightly accumulation/aggregation of highly dispersed, uniform carbon spheres with size between 60 nm and 80 nm. After activation in static air, rich mesopores and micropores were introduced into the spherical particles (Figure S2). The small size of the particles ensures that these mesopores and micropores are short enough to access. The resulting HPCs show BET surface area values as high as 1306 m^2/g and pore volumes up to 1.11 cm^3/g. The mesopore volume can reach even 63.9% of the total pore volume, which was not observed for other activation methods[23]. The materials were investigated as supercapacitor electrode materials. They showed high capacitance and low ESR, demonstrating efficient ion diffusion and effective adsorption of the electrolyte ions. The synthetic method is proved to be universal for monosaccharide, disaccharide and polysaccharide.

Results

Sphere accumulation/aggregation is a nice way to establish porosity. Small spheres have quite a few advantages over the large ones to build mesoporous interparticle voids. However, it is of great challenge to synthesize highly dispersed carbon spheres under 100 nm by bottom-up techniques due to the high surface energy of small particles. Among the reported approaches to fabricate carbon spheres, HTC of biomass is an ideal choice owing to the advantages of low cost and good sustainability[24]. Nevertheless, the serious crosslinking of neighboring spheres during classical HTC of biomass typically leads to the production of nonporous micrometer-sized carbon spheres or clusters with only a little micropores (Figure S3)[25–27]. These large spheres eliminate the possibility of forming mesoporous interparticle voids. As far as we are concerned, there is few reports involving the fabrication of uniform and monodispersed carbon spheres under 100 nm by HTC of biomass[17,22,28]. Here we fabricated uniform carbon spheres with an average size of 70 nm by using commercial kayexalate as the structure-directing agent during the HTC of carbohydrates. We take fructose and glucose as the model substrates first because they are the basic sugar building blocks of biomasses. From a macroscopic view, free-standing carbon monoliths instead of powder were achieved (Figure 1). SEM images demonstrate that the kayexalate-assisted HTC (KAHTC) materials are constructed by dispersed and uniform carbon spheres ranging from 60 nm to 80 nm (Figure 1, Figure S4). The accumulation/aggregation of spheres helps to build the framework of the 3D macro-mesoporous carbon architecture.

In order to investigate the effect of kayexalate on KAHTC products, kayexalate ratios from 0.1 wt% to 2 wt% of saccharide were employed in condition experiments. SEM images show that 0.1 wt% additive is enough to completely alter the morphology of HTC products. When the weight ratio is less than 0.2 wt%, the KAHTC materials are comprised of carbon clusters which are formed by interconnected spherical nanoparticles. When the amount goes to 0.5 wt% or more, dispersed, uniform spherical particles dominate the product (Figure 2). Further increase of kayexalate to 2 wt% leads to formation of syrupy suspension instead of carbon monolith. It illustrates that kayexalate suppresses the crosslinking of carbon particles. N_2 sorption isotherms reveal that both Fru-40-160 and Glu-40-180 exhibit an intermediate shape between type II and IV according to the IUPAC classification with a small hysteresis loop from $P/P_0 = 0.9$ to 1.0, demonstrating the presence of interparticle voids[29,30]. The voids are in the range of 4–200 nm according to the DFT pore size distribution (Figure S5). The BET surface area of KAHTC products is higher than that of classical HTC ones (< 1.0 m^2/g) and rises with the increase of kayexalate amount to approximate 80 m^2/g (Entries 1–5, 11–13, Table 1). It is interesting to note that the introduction of kayexalate does little effect on the HTC yield (Table S1). That is, kayexalate helps to reduce the sphere size without the loss of output. Dispersed and uniform spheres are attained even at the saccharide concentration of 240 g/L (Figure S6).

KOH activation at around 600°C is most frequently applied to import porous structure into the classical HTC materials. Apart from the drawback of massive use of KOH (generally KOH: carbon = 4), the developed structure is almost totally composed of micropores, which is bad for mass transfer[31,32]. The carbonization degree is always too low for electrochemical applications. Heat-treatment under N_2 or Ar atmospheres at 900°C is commonly applied to carbonize HTC materials however with negligible mesopores. We proposed here the new activation process in static air at 900°C. Air was reported to adjust the surface functional groups of HTC materials[33] or activate carbonaceous materials under low temperatures with long reaction time[34], while no examples of activation process by air were presented at such high temperature, which may due to the complete decomposition of the carbonaceous material. According to our experimental data, the activation yield in static air at 900°C is around 23%, comparable to that by KOH activation at 600°C (27%) (Table S2). In fact, no residue was left by KOH activation at 900°C according to our experiment. Different from the KOH activated product and HTC materials carbonized under inert gas protection, the HPCs produced by air activation show rich mesopores throughout nanoscale spheres (Figure 3) and good carbonization is attained at the same time. The minor diameter not only enhances the porosity (mesopores only appear on the surface of carbon spheres with large size, Figure S7) but also ensures that the developed mesopores are short enough to reach. N_2 sorption isotherms strongly support the TEM results. Steep uptakes at low P/P_0 and clear hysteresis loop suggest the coexistence of micropores and mesopores in the obtained HPCs, which is consistent with the DFT pore size distribution (Figure S5)[35]. In contrast, both carbons activated by KOH and N_2 show overlapping adsorption-desorption curves, demonstrating the absence of mesopores (Figure S8). The surface area of Fru-40-900 is as large as 1306 m^2/g and the pore volume reaches 1.01 cm^3/g (Entry 8, Table 1), considerably higher than those previously reported values for hydrothermal carbons or carbogels[17,18,25], KOH activated Fru-40-160, and carbonized Fru-40-160 in N_2 atmosphere (Entry 18, 19, Table 1). The HPCs prepared using other amounts of kayexalate also possess surface areas above 1159 m^2/g and pore volumes over 0.91 cm^3/g with large mesopore volume proportions (Entries 6-9, 14, 15, Table 1). For Glu-40-900, $V_{macro\text{-}meso}/V_{micro}$ can reach as high as 1.77, which is a compelling goal to achieve for HTC-based carbons. When the amount of KAHTC material is increased in the activation process, the surface area and mesopore pore volume of as-obtained HPCs are still high although the mesopore proportion decreases a little due to the insufficient activation of the KAHTC material at the bottom (Entry 10, Table 1). After the activation step, the 3D macro-mesoporous nano-networks were perfectly reserved (Figure S9).

Elemental analysis shows that there is ~17wt% of oxygen atoms in final HPCs (Table S3). Abundant oxygenated functional groups are reserved, indicating that the loss of functionalization is well suppressed during the activation process. XRD analysis in Figure S10a shows only one broad peak for Fru-40-160 and Glu-40-180 around 22° attributed to 002 reflection of hexagonal graphite. After calcination, the peak shifts towards 23.6° implying a decrease in the interlayer spacing[36]. A peak centered at 43° emerges which is the equivalent of 100 reflection, exemplifying better graphitization[37,38]. These results manifest that the activation process results in carbonization together with rich meso-micropores at the same time. No observed signals for S or Na appear in X-ray photoelectron spectroscopy (XPS), which indicates that little S or Na residues is in the

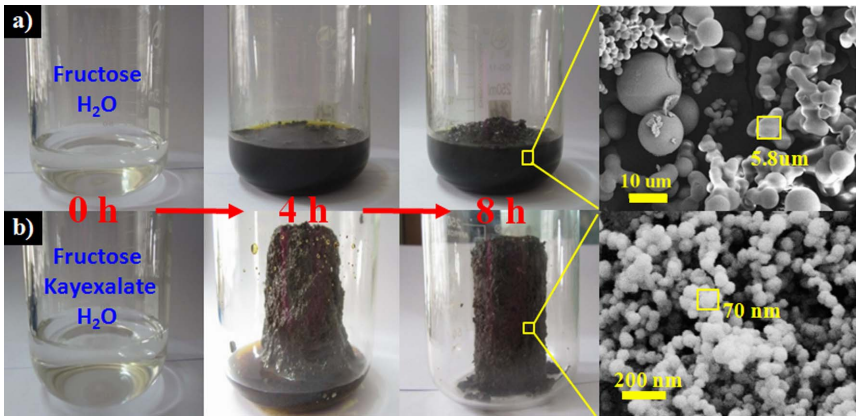

Figure 1 | **Illustration of KAHTC process compared to classical HTC of fructose.**

carbon architecture (Figure S10b). High resolution XPS demonstrates that the carbon atoms in Fru-40-900 exist mainly in the form of C-C/C=C and CHx (284.6 eV)[18]. The others bind with oxygen atoms as –C-O (285.7 eV) and >C=O (287.3 eV) (Figure S10c)[39]. The O envelope demonstrates that the oxygen are mainly in the form of quinone, esters, anhydrides and phenol (Figure S10, d,e)[40]. Raman spectra in Figure S11 show two overlapping bands at 1360 cm^{-1} and 1600 cm^{-1} for both Fru-40-900 and Glu-40-900. The G band at 1600 cm^{-1} indicates the presence of C sp2 atoms in aromatic and olefinic molecules[41]. The D band centered at 1360 cm^{-1} is assigned to the ring-breathing vibrations in benzene or condensed benzene ring in amorphous HPCs[39].

The HPCs were taken as supercapacitor materials to probe into their capacitive performance and diffusion efficiency. They show good electronic conductivity and we didn't add any other conductive additives (*e.g.* acetylene black) in the working electrode (Table S4). The performance of Fru-40-900 was set as an example and evaluated by CV as well as galvanostatic charge-discharge measurements in 6M KOH. The CV curves show quasi-rectangular shape at scanning rate from 20 mv/s to 500 mv/s, demonstrating a typical characteristic of double-layer capacitance (Figure 4a). The galvanostatic charge/discharge curves reveal almost symmetrical triangle without obvious voltage drop (IR) related to the internal resistance during the changing of polarity (Figure 4b), suggesting the fast transmission of ions in the hierarchically porous structure. The specific capacitance was calculated from the discharge curves with values of 170 F/g at current density of 0.1 A/g and the capacity decays little from 0.1 A/g to 1 A/g (>160 F/g). Capacitance of 140 F/g is maintained at the current density of 10 A/g (Figure S12), which manifests that Fru-40-900 has excellent electrolyte accessibility attributed to less microporosity[16]. The capacitance is comparable to nitrogen-doped HTC carbons with BET surface area above 2000 m^2/g, suggesting the more efficient use of adsorption sites[23]. EIS test was also carried out to understand the capacitive behavior of Fru-40-900 over the frequency range of 100 kHz to 0.1 Hz. The sufficient ion diffusion is confirmed by the nyquist plot (Figure 4c). The low-frequency segment is nearly perpendicular, indicating a nearly ideal capacitive behavior. The nyquist plot shows a short Warburg-type line, which is another evidence of the fast ion transfer in Fru-40-900. The ESR is estimated to be 0.08 Ω by the diameter of the semicircle at the real axis, indicating superior conductivity. The efficient ion transfer results from the specific porous structure. The electrolyte ions are stored in the macro-mesopores constructed by the accumulation/aggregation of nanospheres before charging. They can directly move into the short meso-micropores in the spheres when charging without the diffusion steps from the bulk solution (Scheme S1). Figure 4d reveals the cycling stability at a constant current density of 10 A/g. The Fru-40-900 sample displays a 12.8% decrease of capacitance after 10000 cycles, which is attributed to the pesudocapacitance arising from the oxygenated functional groups.

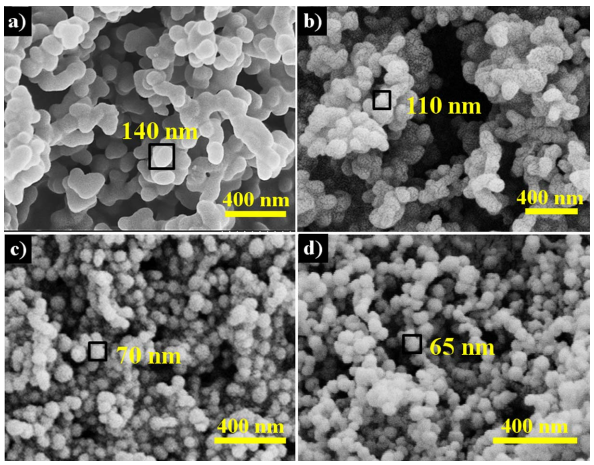

Figure 2 | **SEM images of Fru-8-160 (a), Fru-16-160 (b), Fru-40-160 (c) and Fru-80-160 (d); Kayexalate: Fructose= 0.1%, 0.2%, 0.5%, 1.0% by weight.**

In the view of economy, disaccharide and polysaccharide are more competitive to commercialize. Therefore, we also investigate the kaxeyalate-assisted HTC course of sucrose and α-cellulose. Considering that cellulose is difficult to hydrolyze, the HTC temperature was lifted to 230°C and the reaction time was extended to 24 h[42]. After activation, the morphologies are similar to the carbon networks fabricated by monosaccharide (fructose or glucose). Surface areas larger than 1100 m^2/g and pore volumes over 0.79 cm^3/g were obtained for both Cel-40-900 and Suc-40-900 (Entries 16, 17, Table 1). Slightly different from others, the nanospheres in Cel-40-900 are not that uniform however the sphere size is still much smaller than 200 nm (Figure S13). The above information demonstrates that the KAHTC and air activation methods are universal for the production of HPCs from carbohydrates.

Discussion

It is important to understand the formation mechanism of the small spherical particles during the KAHTC process. We tried to get some inspiration from the zeta potentials of the intermediate products. It has long been recognized that zeta (ζ) potential is a good index of the magnitude of the repulsive interaction between colloidal particles and it is commonly used to access the stability of colloidal and particle size[43]. Four KAHTC processes with 0, 16, 80, 160 mg of kayexalate and 8 g of fructose were conducted at 160°C for 2 hours. The obtained colloids were used for ζ potential tests and the results were

Table 1 | Textual properties of the prepared materials

Entry	Carbons	S_{BET}[a] (m^2/g)	Vmicro (cm^3/g)	Vmacro-meso (cm^3/g)	Vtotal (cm^3/g)	PS[b] (nm)
1	Fru-160	<1.0	--	--	0.01	---
2	Fru-8-160	19.9	0.007	0.013	0.020	15.9
3	Fru-16-160	29.1	0.008	0.026	0.034	11.3
4	Fru-40-160	52.2	0.011	0.067	0.078	11.1
5	Fru-80-160	77.1	0.013	0.147	0.16	15.0
6	Fru-8-900	1287	0.48	0.49	0.97	4.2
7	Fru-16-900	1183	0.49	0.49	0.98	4.0
8	Fru-40-900	1306	0.45	0.56	1.01	4.5
9	Fru-80-900	1159	0.56	0.41	0.97	5.5
10[c]	Fru-40-900	1228	0.51	0.35	0.86	3.8
11	Glu-180	<5	--	--	0.01	1.5
12	Glu-16-180	48.8	0.011	0.053	0.064	9.2
13	Glu-40-180	78.6	0.01	0.22	0.23	29.1
14	Glu-16-900	1165	0.42	0.49	0.91	3.7
15	Glu-40-900	1276	0.40	0.71	1.11	5.0
16	Cel-40-900	1154.5	0.39	0.59	0.98	5.35
17	Suc-40-900	1129.2	0.42	0.37	0.79	4.39
18	Fru-40-900N	446.4	0.19	0.05	0.24	---
19	Fru-40-KOH	655.1	0.29	0.04	0.33	---

[a] Specific surface area from BET method. [b] BJH pore size [c] 3 g of Fru-40-160 was activated in a 100 ml crucible.

summarized in Figure 5a. For accuracy, every ζ potential test was repeated for six times. The average ζ potentials are -29.2, -37.5, -39.6, -44.2 mV, respectively. The difference suggests that the surface of carbon nanospheres become more negatively charged with the addition of kayexalate. The negatively charged nanoparticles would repel each other and protect them from crosslinking (Figure 5b). The size distributions of the colloidal particles according to DLS tests were summarized in Figure S14b. The sample without kayexalate shows a broad size distribution from hundred nanometers to several micrometers while the nanoparticles of the KAHTC products prove to be much more uniform with an average size of 160 nm. It is larger than the size of carbon spheres measured from SEM and TEM. This difference implies that there is a negatively charged layer on the carbon particle surface. In this system, the layer is surely composed of polystyrene sulfonate anion. Figure S14a reveals the size distribution of kayexalate micelles. The micelles vary from less than 10 nanometers to several micrometers, which are absolutely different from the size of the carbon particles. Furthermore, the micelles are always not stable at high temperatures[9]. Therefore, the possibility of kayexalate acting as a soft template is excluded. IR spectra reveal the same surface features of Fru-160 and Fru-40-160 (Figure S15), implying the similar polymerization process during which saccharides dehydrated to HMF followed by the nucleation and growing course[39,44]. Thus, we deem that the KAHTC process undergoes mainly two procedures: nucleation of dehydrated saccharides and adsorption of kayexalate on carbon spheres (Figure 5b).

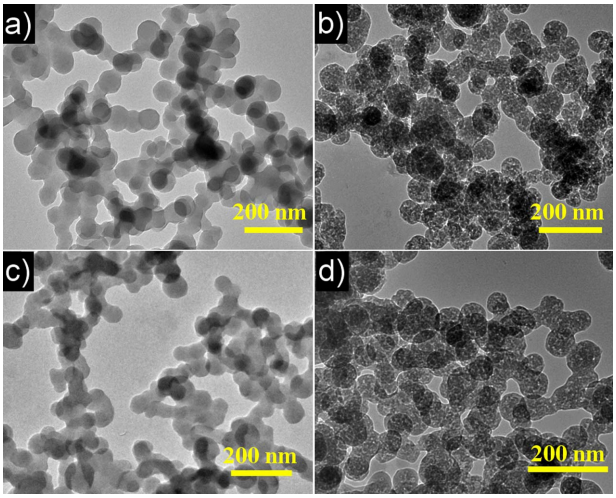

Figure 3 | TEM image of Fru-40-160 and Glu-40-180 before (a,c) and after (b, d) air activation.

The mesopores and micropores introduced during the activation step can be explained by the reaction between carbon atoms and air. TG-MS results show that the weight loss is slow and there is only CO_2 produced in Ar atmosphere due to the reaction between carbon and oxygen atoms in the KAHTC material matrix. While in air, KAHTC material reacts with air very fast and produces CO_2 and CO at the same time. The carbon completely decomposes before 500°C (Figure S16). The reaction between carbon atoms and air would give rise to the formation of micropores and micropore collapse, resulting in high mesopore ratio. In contrast to the flowing air used in TG-MS analysis, the static and limited air condition applied for the practical activation process prevents the KAHTC material from complete decomposition and thus leads to high carbon yield.

In summary, we designed and fabricated a series of hierarchically porous carbon materials via a facile, improved HTC method followed by air activation. The HPCs consisted of two parts: the outer 3D macro-mesopores serve as buffering reservoirs minimizing diffusion distance and the inner short-range meso-micropores supply adsorption sites and efficient transport pathways. The high capacitance and low ESR as supercapacitor electrode material verify the effective adsorption and fast transmission of electrolyte ions in the hierarchically porous structure. The method is proved to be general for carbohydrates including monosaccharides, disaccharide, and polysaccharide.

Methods

Materials. D-(+)-fructose, D-(+)-glucose, sucrose and α-cellulose were purchased from Aladdin industrial corporation. Kayexalate was purchased from Sigma-Aldrich. All other chemicals were of analytical purity if not otherwise noted.

Materials synthesis. In a typical synthetic process, 8 g of D-fructose (D-glucose, sucrose) and desired amount of kayexalate were dissolved in 50 mL of water. Then the solutions were transferred into a Teflon-lined autoclave and sealed. The autoclave was put into a temperature-programming oven and heated to 160°C (180°C for glucose and sucrose) and maintained for 8 hours. Dark-brown monoliths were obtained and then they were washed several times with water and ethanol. After filtration, the materials were dried under 80°C in the air. These materials were named Fru-x-y, Glu-x-y and Suc-x-y (x stands for the amount of kayexalate in milligrams, y was the reaction temperature). The samples without addition of kayexalate were named Fru-160 and Glu-180, respectively. In the case of cellulose, 4 g of cellulose was applied. The HTC temperature and time were extended to 230°C and 24 hours, respectively.

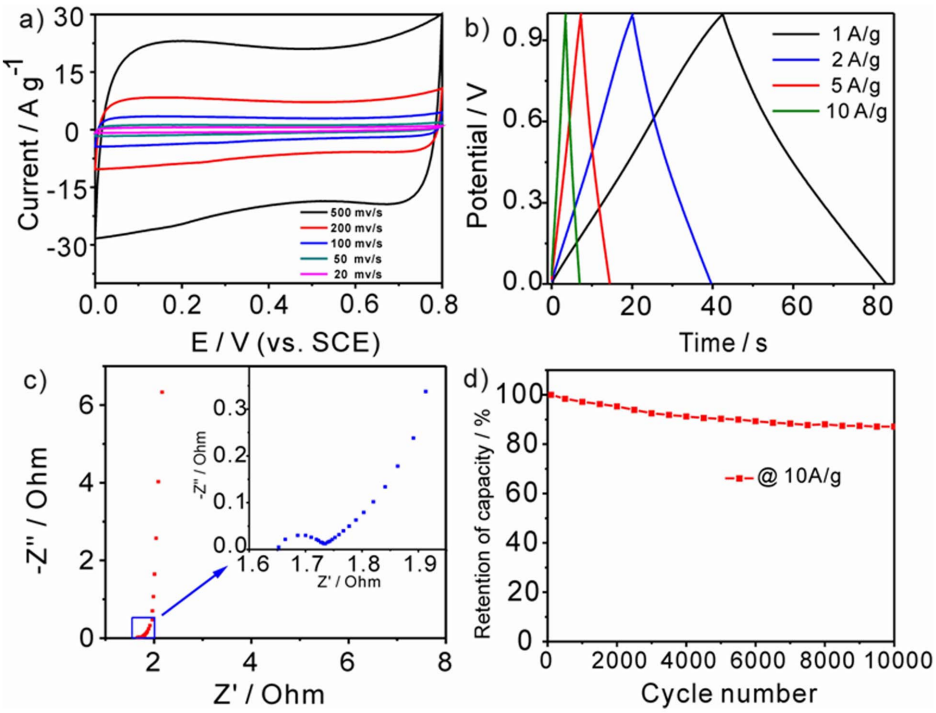

Figure 4 | **Cyclic voltammograms (a), galvanostatic charge/discharge curves measured at various current densities (b), nyquist plot of electrochemical impedance (c) and variations of the specific capacitance versus cycle number (at the current density of 10 A/g) (d) of Fru-40-900 in 6 M KOH.**

In a typical activation process, 1 g of the obtained KAHTC materials were put into a crucible with a lid and calcined at 900°C for 1 h in a Nabertherm L3/11 muffle oven. The oven is connected to the external environment, which ensures that the furnace is full of air. The obtained HPCs were denoted as Fru-x-900, Glu-x-900, Suc-x-900 and Cel-x-900 (x is the amount of kayexalate in milligrams, 900 represents the activation temperature). For comparison, the Fru-40-160 was also activated by KOH and carbonized in N_2. During KOH activation, 1 g of Fru-40-160 was mixed with 4 g of KOH and heated at 600°C in N_2 for 1 hour, respectively. After calcination, the obtained materials were washed with 2 M HCl, dried at 80°C in the air, and named Fru-40-KOH. During N_2 activation, 1 g of Fru-40-160 was transfer into a crucible with a lid and heated at 900°C under the protection of N_2 (400 mL/min). The resulting carbon material was named Fru-40-900 N.

Characterization. Scanning electron microscope (SEM, LEO 1550) was applied to characterize the morphology of the carbon materials. Transmission electron microscope (TEM) images were obtained from a Hitachi H7700 transmission electron microscope with CCD imaging system on an acceleration voltage of 100 kV. N_2 adsorption analysis was performed at 77 K using a Micromeritics ASAP 2020 to access the surface area and pore distribution. All the samples were outgassed at 200°C for 12 h. Then adsorption-desorption processes were conducted between the relative pressure (P/P_0) range of 10^{-6}-1. The specific surface area was calculated by the conventional Brunauere-Emmette-Teller (BET) method. The pore size distribution (PSD) plot was recorded by the DFT model. The micropore volume (V_{micro}) was estimated by using the t-plot method. The diffraction data were collected at room temperature with 2 θ scan range between 5° and 90° using a wide-angle X-ray diffraction (Model D/tex-Ultima TV, 1.6 kV, Rig-aku, Japan) equipped with Cu Ka radiation (1.54 Å). The X-ray photoelectron spectra (XPS) information was accessed by a ESCALAB_250Xi instrument using a magnesium anode (Mg 1253.6 eV) X-ray source. The zeta potential tests were carried out at Malvern ZEN3600 instrument. The TG-MS was carried out at Ar and air (Ar replacing N_2) by a ramping temperature of 10°C/min.

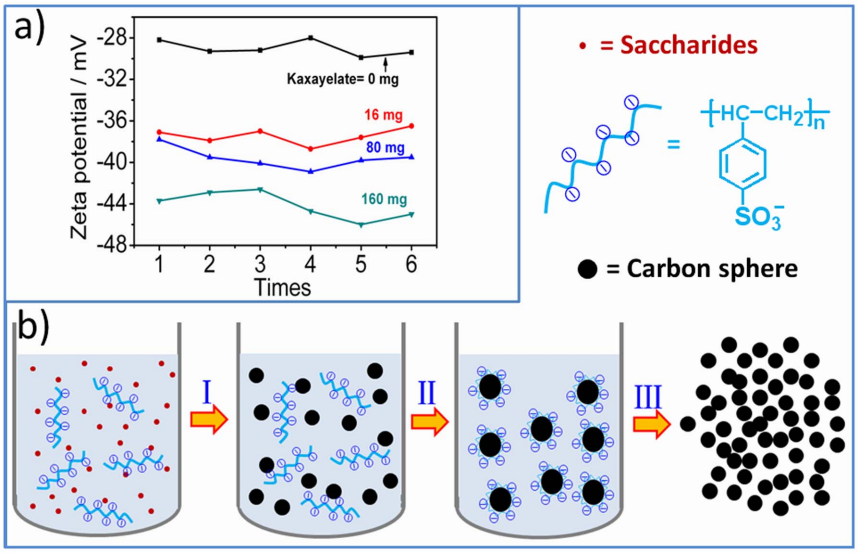

Figure 5 | **Zeta potentials of the colloidal particles prepared by HTC processes with different amount of kayexalate (a) and proposed mechanism for the KAHTC process (b).**

Electrochemical tests. The supercapacitive properties of the HPCs were investigated by CV curves at different scan rates and galvanostatic charge/discharge. These measurements were carried out in a two-electrode system in 6 M KOH. The work electrode was prepared by mixing 5 mg of the prepared HPCs with 2 mL water, 400 ul ethanol and 100 ul nafion. Then 25 ul of the ink was dropped onto a glassy carbon electrode. The real mass of the materials on the electrode was weighed after drying. All the data was collected by a Gamry reference 600 workstation.

1. Joo, S. H. *et al.* Ordered nanoporous arrays of carbon supporting high dispersions of platinum nanoparticles. *Nature* **412**, 169–172 (2001).
2. Liang, C., Li, Z. & Dai, S. Mesoporous Carbon Materials: Synthesis and Modification. *Angew. Chem. Int. Ed.* **47**, 3696–3717 (2008).
3. Morris, R. E. & Wheatley, P. S. Gas Storage in Nanoporous Materials. *Angew. Chem. Int. Ed.* **47**, 4966–4981 (2008).
4. Dai, L. M., Chang, D. W., Baek, J. B. & Lu, W. Carbon Nanomaterials for Advanced Energy Conversion and Storage. *Small* **8**, 1130–1166 (2012).
5. Ryoo, R., Joo, S. H. & Jun, S. Synthesis of Highly Ordered Carbon Molecular Sieves via Template-Mediated Structural Transformation. *J. Phys. Chem. B* **103**, 7743–7746 (1999).
6. Zhai, Y. P. *et al.* Carbon Materials for Chemical Capacitive Energy Storage. *Adv. Mater.* **23**, 4828–4850 (2011).
7. Li, Q. *et al.* Synthesis of mesoporous carbon spheres with a hierarchical pore structure for the electrochemical double-layer capacitor. *Carbon* **49**, 1248–1257 (2011).
8. Wei, J. *et al.* A Controllable Synthesis of Rich Nitrogen-Doped Ordered Mesoporous Carbon for CO2 Capture and Supercapacitors. *Adv. Funct. Mater.* **23**, 2322–2328 (2013).
9. Kubo, S., White, R. J., Yoshizawa, N., Antonietti, M. & Titirici, M. M. Ordered Carbohydrate-Derived Porous Carbons. *Chem. Mater.* **23**, 4882–4885 (2011).
10. Fang, Y. *et al.* A Low-Concentration Hydrothermal Synthesis of Biocompatible Ordered Mesoporous Carbon Nanospheres with Tunable and Uniform Size. *Angew. Chem. Int. Ed.* **49**, 7987–7991 (2010).
11. Wang, D. W., Li, F., Liu, M., Lu, G. Q. & Cheng, H. M. 3D aperiodic hierarchical porous graphitic carbon material for high-rate electrochemical capacitive energy storage. *Angew. Chem. Int. Ed.* **47**, 373–376 (2008).
12. Zhu, Y. W. *et al.* Carbon-Based Supercapacitors Produced by Activation of Graphene. *Science* **332**, 1537–1541 (2011).
13. Sun, J. M. *et al.* Macro-mesoporous silicas complex and the carbon replica. *Micropor. Mesopor. Mater.* **100**, 356–360 (2007).
14. Guo, D. C. *et al.* Ionic liquid C(16)mimBF(4) assisted synthesis of poly(benzoxazine-co-resol)-based hierarchically porous carbons with superior performance in supercapacitors. *Energ. Environ. Sci.* **6**, 652–659 (2013).
15. Huang, Y. *et al.* One-step hydrothermal synthesis of ordered mesostructured carbonaceous monoliths with hierarchical porosities. *Chem. Commun.* 2641–2643 (2008).
16. Huang, C.-H. *et al.* Three-Dimensional Hierarchically Ordered Porous Carbons with Partially Graphitic Nanostructures for Electrochemical Capacitive Energy Storage. *ChemSusChem* **5**, 563–571 (2012).
17. Fellinger, T. P., White, R. J., Titirici, M. M. & Antonietti, M. Borax-Mediated Formation of Carbon Aerogels from Glucose. *Adv. Funct. Mater.* **22**, 3254–3260 (2012).
18. White, R. J., Yoshizawa, N., Antonietti, M. & Titirici, M. M. A sustainable synthesis of nitrogen-doped carbon aerogels. *Green Chem.* **13**, 2428–2434 (2011).
19. Xue, C., Tu, B. & Zhao, D. Facile fabrication of hierarchically porous carbonaceous monoliths with ordered mesostructure via an organic organic self-assembly. *Nano Res.* **2**, 242–253 (2009).
20. Huang, C.-h., Doong, R.-a., Gu, D. & Zhao, D. Dual-template synthesis of magnetically-separable hierarchically-ordered porous carbons by catalytic graphitization. *Carbon* **49**, 3055–3064 (2011).
21. Bloss, P., Hergeth, W. D., Doring, E., Witkowski, K. & Wartewig, S. Association of Polyoxyethylene-polyoxypropylene Block Copolymers in Aqueous-solutions. *Acta Polym.* **40**, 260–265 (1989).
22. Liu, J. *et al.* A facile soft-template synthesis of mesoporous polymeric and carbonaceous nanospheres. *Nat Commun* **4** (2013).
23. Sevilla, M. *et al.* Hydrothermal synthesis of microalgae-derived microporous carbons for electrochemical capacitors. *J. Power Sources* **267**, 26–32 (2014).
24. Sun, X. M. & Li, Y. D. Colloidal carbon spheres and their core/shell structures with noble-metal nanoparticles. *Angew. Chem. Int. Ed.* **43**, 597–601 (2004).
25. Titirici, M. M., Antonietti, M. & Baccile, N. Hydrothermal carbon from biomass: a comparison of the local structure from poly- to monosaccharides and pentoses/hexoses. *Green Chem.* **10**, 1204–1212 (2008).
26. Titirici, M. M. & Antonietti, M. Chemistry and materials options of sustainable carbon materials made by hydrothermal carbonization. *Chem. Soc. Rev.* **39**, 103–116 (2010).
27. Hu, B. *et al.* Engineering Carbon Materials from the Hydrothermal Carbonization Process of Biomass. *Adv. Mater.* **22**, 813–828 (2010).
28. Zhang, P. F. *et al.* Improving Hydrothermal Carbonization by Using Poly(ionic liquid)s. *Angew. Chem. Int. Ed.* **52**, 6028–6032 (2013).
29. Tao, Y. S., Kanoh, H., Abrams, L. & Kaneko, K. Mesopore-modified zeolites: Preparation, characterization, and applications. *Chem. Rev.* **106**, 896–910 (2006).
30. Wattanakit, C. *et al.* The versatile synthesis method for hierarchical micro- and mesoporous zeolite: An embedded nanocarbon cluster approach. *Can. J. Chem. Eng.* **90**, 873–880 (2012).
31. Zhao, L. *et al.* Nitrogen-Containing Hydrothermal Carbons with Superior Performance in Supercapacitors. *Adv. Mater.* **22**, 5202–5206 (2010).
32. Sevilla, M. & Fuertes, A. B. Sustainable porous carbons with a superior performance for CO2 capture. *Energ. Environ. Sci.* **4**, 1765–1771 (2011).
33. Zhang, Z. B. *et al.* Removal of uranium(VI) from aqueous solutions by carboxyl-rich hydrothermal carbon spheres through low-temperature heat treatment in air. *J. Radioanal. Nucl. Chem.* **298**, 361–368 (2013).
34. Inagaki, M., Park, C. R., Skowronski, J. M. & Morawski, A. W. Glass-like Carbon Spheres - Activation, Porosity and Application Possibilities. *Adsorpt. Sci. Technol.* **26**, 735–787 (2008).
35. Chen, L. F. *et al.* Synthesis of Nitrogen-Doped Porous Carbon Nanofibers as an Efficient Electrode Material for Supercapacitors. *Acs Nano* **6**, 7092–7102 (2012).
36. Jin, Y. Z. *et al.* High temperature annealing effects on carbon spheres and their applications as anode materials in Li-ion secondary battery. *Carbon* **44**, 724–729 (2006).
37. Eckert, H., Levendis, Y. A. & Flagan, R. C. Glassy Carbons from Poly(furfuryl alcohol) Copolymers - Structural Studies by High-Resolution Solid-State NMR Techniques. *J. Phys. Chem.* **92**, 5011–5019 (1988).
38. Zhao, L. *et al.* Sustainable nitrogen-doped carbonaceous materials from biomass derivatives. *Carbon* **48**, 3778–3787 (2010).
39. Sevilla, M. & Fuertes, A. B. Chemical and Structural Properties of Carbonaceous Products Obtained by Hydrothermal Carbonization of Saccharides. *Chem.-Eur. J.* **15**, 4195–4203 (2009).
40. Figueiredo, J. L., Pereira, M. F. R., Freitas, M. M. A. & Órfão, J. J. M. Modification of the surface chemistry of activated carbons. *Carbon* **37**, 1379–1389 (1999).
41. Ferrari, A. C. & Robertson, J. Interpretation of Raman spectra of disordered and amorphous carbon. *Phys. Rev. B* **61**, 14095–14107 (2000).
42. Sevilla, M. & Fuertes, A. B. The production of carbon materials by hydrothermal carbonization of cellulose. *Carbon* **47**, 2281–2289 (2009).
43. Ofir, E., Oren, Y. & Adin, A. Electroflocculation: the effect of zeta-potential on particle size. *Desalination* **204**, 33–38 (2007).
44. Falco, C. *et al.* Hydrothermal Carbon from Biomass: Structural Differences between Hydrothermal and Pyrolyzed Carbons via C-13 Solid State NMR. *Langmuir* **27**, 14460–14471 (2011).

Acknowledgments

Financial support from the National Natural Science Foundation of China (21376208 & U1162124), the Zhejiang Provincial Natural Science Foundation for Distinguished Young Scholars of China (LR13B030001), the Specialized Research Fund for the Doctoral Program of Higher Education (J20130060). The Fundamental Research Funds for the Central Universities, the Program for Zhejiang Leading Team of S&T Innovation, and the Partner Group Program of the Zhejiang University and the Max-Planck Society are greatly appreciated.

Author contributions

Y.T.G. and Y.W. conceived and designed the experiments. Y.T.G. performed all the experiments and analyzed all the data. Z.Z.W. and J.W. helped analyze the XPS data. Y.T.G. and Y.W. co-wrote the paper. P.F.Z. and H.R.L. discussed the results and commented on the manuscript.

Additional information

Supplementary information accompanies this paper at http://www.nature.com/scientificreports

Competing financial interests: The authors declare no competing financial interests.

How to cite this article: Gong, Y. *et al.* Design and Fabrication of Hierarchically Porous Carbon with a Template-free Method. *Sci. Rep.* **4**, 6349; DOI:10.1038/srep06349 (2014).